JBC Papers in Press. Published on August 31, 2013 as Manuscript M113.501585
The latest version is at http://www.jbc.org/cgi/doi/10.1074/jbc.M113.501585

The Structural Basis for Phospholamban Inhibition of the Calcium Pump in Sarcoplasmic Reticulum

Brandy L. Akin[‡1], Thomas D. Hurley[§], Zhenhui Chen[‡], and Larry R. Jones[‡2]

From the [‡]Krannert Institute of Cardiology and the Department of Medicine, and the [§]Department of Biochemistry and Molecular Biology, Indiana University School of Medicine, Indianapolis, IN 46202

*Running title: *Crystal Structure of the PLB4/SERCA Complex*

Keywords: phospholamban, SERCA, calcium ATPase, protein crystallization, protein cross-linking, calcium transport, sarcoplasmic reticulum (SR), sarcolipin, crystal structure

Background: PLB regulates SERCA activity and is thus a key regulator cardiac contractility.
Results: We present the crystal structure of SERCA in complex with PLB at 2.8 Å resolution.
Conclusion: PLB stabilizes a divalent cation-free conformation of SERCA with collapsed Ca^{2+} binding sites. We call the structure *E*2-PLB.
Significance: The *E*2-PLB structure explains how PLB decreases Ca^{2+} affinity and depresses cardiac contractility.

ABSTRACT

P-type ATPases are a large family of enzymes that actively transport ions across biological membranes by interconverting between high (*E*1) and low (*E*2) ion-affinity states; these transmembrane transporters carry out critical processes in nearly all forms of life. In striated muscle, the archetype P-type ATPase, SERCA (sarco(endo)plasmic reticulum Ca^{2+}-ATPase), pumps contractile-dependent Ca^{2+} ions into the lumen of sarcoplasmic reticulum, which initiates myocyte relaxation and refills the sarcoplasmic reticulum in preparation for the next contraction. In cardiac muscle, SERCA is regulated by phospholamban (PLB), a small inhibitory phosphoprotein that decreases the Ca^{2+} affinity of SERCA and attenuates contractile strength. cAMP-dependent phosphorylation of PLB reverses Ca^{2+}-ATPase inhibition with powerful contractile effects. Here we present the long sought crystal structure of the PLB/SERCA complex at 2.8 Å resolution. The structure was solved in the absence of Ca^{2+} in a novel detergent system employing alkyl mannosides. The structure shows PLB bound to a previously undescribed conformation of SERCA in which the Ca^{2+} binding sites are collapsed and devoid of divalent cations (*E*2-PLB). This new structure represents one of the key unsolved conformational states of SERCA and provides a structural explanation for how dephosphorylated PLB decreases Ca^{2+} affinity and depresses cardiac contractility.

Phospholamban (PLB)[3], a single-span membrane protein of only 52 amino acids, is the principal membrane protein in the heart phosphorylated in response to β-adrenergic stimulation and a critical regulator of cardiac contractile strength (1). In the dephosphorylated state, PLB decreases cardiac contractility by inhibiting the activity of the sarco(endo)plasmic reticulum Ca^{2+}-ATPase (SERCA), an 110-kilodaltaon membrane protein with 10 membrane-spanning segments. PLB inhibits SERCA activity by decreasing Ca^{2+} affinity at its two Ca^{2+} binding sites (I and II) located in the SR membrane, thereby attenuating SR Ca^{2+} filling and contractile force development. Phosphorylation of PLB at Ser^{16} and Thr^{17} partially reverses PLB induced alterations in Ca^{2+} affinity, substantially augmenting contractility (2-4).

Chemical cross-linking was used previously to localize the PLB binding site on SERCA to a groove formed between transmembrane helices M2, M4, M6 and M9 of the Ca^{2+} pump (5-9). In conjunction with functional assays, these cross-linking studies led

This is the author's manuscript of the article published in final edited form as:
Akin, B. L., Hurley, T. D., Chen, Z., & Jones, L. R. (2013). The structural basis for phospholamban inhibition of the calcium pump in sarcoplasmic reticulum. Journal of Biological Chemistry, 288(42), 30181-30191.
http://dx.doi.org/10.1074/jbc.M113.501585

Copyright 2013 by The American Society for Biochemistry and Molecular Biology, Inc.

us to postulate that PLB binds to a unique Ca^{2+}-free (*E*2) state of SERCA and decreases the Ca^{2+} affinity of the enzyme through direct effects on the Ca^{2+} binding sites (5). Recently, a gain-of-function, cross-linkable PLB mutant, PLB4 (N27A, N30C, L37A, V49G-PLB) (Fig. 1), was developed (10) and shown to bind to the Ca^{2+}-ATPase with exceedingly high affinity, comparable to or even greater than that of thapsigargin (TG), the well-known, irreversible Ca^{2+}-ATPase inhibitor (11, 12). Here, we took advantage of PLB4 to stabilize the Ca^{2+}-free state of SERCA and to crystallize it in complex with PLB. The 2.8 Å resolution structure, crystallized in nonyl maltoside, reveals a previously unresolved conformational state of the Ca^{2+} pump captured by PLB, which we define as *E*2-PLB. Importantly, the structure of *E*2-PLB is incompatible with Ca^{2+} (or Mg^{2+}) binding to the enzyme, and confirms hypothesis that mutually exclusive binding of PLB and Ca^{2+} to SERCA is the mechanism by which PLB decreases apparent Ca^{2+} affinity (5).

EXPERIMENTAL PROCEDURES

Protein Preparation—SR vesicles sedimenting at 45,000 x *g* were isolated from rabbit back and hind leg muscle as described previously for cardiac SR vesicles (13). SR vesicle pellets were extracted with 0.6 M KCl, 20 mM MOPS (pH 7.0), resuspended in 0.25 M sucrose, 20 mM MOPS (pH 7.2), and stored frozen in small aliquots at -40°C at a protein concentration of 30 mg/ml. Recombinant WT-PLB and PLB4 were expressed and purified from Sf21 insect cells using anti-PLB monoclonal antibody (2D12) affinity-chromatography as previously described (14). Purified PLB was eluted from the column in 0.1% decyl maltoside or 0.01% dodecyl maltoside (Anatrace), which in control experiments were determined to be optimal detergents for co-crystallization of PLB with the solubilized Ca^{2+}-pump. The purified, eluted PLB proteins were concentrated 100-fold with an Amicon concentrator, and then exhaustively dialyzed against 20 mM MOPS (pH 7.2), 20% glycerol, and 0.1 % decyl maltoside or 0.01% dodecyl maltoside. The final working concentrations of PLB were 8-10 mg protein/ml. PLB was stored frozen at -40°C. Protein concentrations were determined by the Lowry method.

The Ca^{2+} pump suitable for crystallization was solubilized directly from SR vesicles without prior purification or extraction of SR vesicles with low concentrations of deoxycholate (15). Thawed SR vesicles were diluted 1:1 to a protein concentration of 15 mg/ml in buffer containing 2% nonyl maltoside (Anatrace), 20% glycerol, 100 mM MOPS (pH 7.0), 0.12 M sucrose, 80 mM KCl, 3 mM $MgCl_2$, and 2.8 mM EGTA (final concentrations). The samples were allowed to stand for 7 min at room temperature, then ultracentrifuged at 4°C at 100,000 rpm for 15 min in a Beckman TLA 100.1 rotor. The supernatant was collected and PLB was added from the concentrated working solutions at a ratio of 0.14 mg PLB/ 1.0 mg of solubilized SR vesicle protein, determined in control experiments to be a saturating concentration of PLB for inhibition of Ca^{2+}-ATPase activity by lowering apparent Ca^{2+} affinity. This amount of added PLB gave a molar ratio of PLB to SERCA of 2.9:1, as determined by quantitative immunoblotting (16). Final volumes of mother liquors were adjusted by addition of 20% glycerol to make the final EGTA concentration 2 mM and samples were stored at 4°C. Ca^{2+}-ATPase prepared by this method (in 2 mM EGTA) retained 95-100% of the initially solubilized activity for at least 3 weeks at 4° in the presence and absence of PLB (Fig. 2*B*). In pilot studies, the Ca^{2+} pump was solubilized from SR vesicles using other detergents, including $C_{12}E_8$ and octyl glucoside. Solubilization conditions were identical to that described above, using 2% detergent concentrations (Fig. 2*B*).

Crystallization—One day after initial Ca^{2+}-ATPase solubilization and addition of PLB, mother liquors were sedimented a second time by ultracentrifugation as described above. Hanging drops were made by mixing 1 µl of the sedimented mother liquors with 1 µl reservoir solution (15 % glycerol, 17% (W/V) PEG-2000, 200 mM NaOAc, and 5 mM β-mercaptoethanol) and crystals were grown by vapor diffusion at 4°C. Single crystals appeared within 2 weeks and grew to a final size of 150 x 100 x 50 µm within a month. Crystals were mounted using nylon fiber loops and flash cooled in liquid nitrogen with no additional cryo-protectant.

Data Collection, Structure Solution and Refinement—The X-ray diffraction data were collected at Beamline 19-ID operated by the Structural Biology Center at the Advanced Photon Source within Argonne National Laboratory. All diffraction data were collected at a wavelength of 0.979 Å from a single crystal at 100°K. The crystal was formed from PLB4 added in decyl maltoside. The diffraction data was integrated and scaled using the program package HKL3000 (17). The structure was solved by molecular replacement using the individual protein domains of SERCA (PDB ID 2C8L) (18) as the search models. Solutions were found for the three cytoplasmic domains using Phaser (19), but no solution for the transmembrane region was obtained. The initial model was constructed from the three cytoplasmic domains and used to calculate initial electron density maps into which the individual transmembrane helices were manually fit using the program Coot (version 0.6.1(20)) and the connectivity of the M4 and M5 helices to one of the cytoplasmic domains and the C-terminal transmembrane helix as points of reference. Helix M4 required fitting as two distinct sections and the connecting polypeptide was manually fit to the electron density in Coot. The structure was subjected to interative rounds of model building and refinement using the program Refmac5 (21) and included the use of TLS tensors (22) to model the anisotropy of the individual domains and PLB. In addition to SERCA and PLB, the final model includes one potassium ion and 2 non-covalently associated maltose molecules, for which the acyl chains were not visible in the electron density and hence have been modeled simply as maltose residues. Initial attempts to include a magnesium ion bound to site I in the transmembrane domain gave rise to a negative difference peak at 4.2 sigma in the F_o-F_c electron density map at the position of the modeled magnesium ion. Based on this information, combined with the lack of a positive peak in the F_o-F_c electron density map greater than 2.7 sigma when the model is refined in the absence of magnesium and the fact that magnesium ions are not required for PLB cross-linking, we conclude that the PLB/SERCA complex lacks metal ions bound to the transmembrane metal sites.

Ca^{2+}-ATPase Assay—Ca^{2+}-ATPase activity was determined colorimetrically by measuring inorganic phosphate release from ATP (16). 12 µg of solubilized Ca^{2+}-ATPase protein (taken from mother liquors used for protein crystallization) were added to 1 ml of ATPase buffer containing 50 mM MOPS (pH 7.0), 3 mM $MgCl_2$, 3 mM ATP, 100 mM KCl, 1 mM EGTA, 5 mM NaN_3, and 3 µg/ml A23187. Ionized Ca^{2+} concentrations were set by addition of $CaCl_2$. Some reaction tubes in addition contained 60-80 µg of anti-PLB 2D12 antibody to reverse PLB inhibition of Ca^{2+}-ATPase activity (23). Reactions were conducted at 37°C and Ca^{2+}-dependent activities are reported. K_{Ca} values designate Ca^{2+} concentrations at which Ca^{2+}-ATPase is half-maximally activated.

Cross-linking—Cross-linking assays were conducted with solubilized Ca^{2+}-ATPase protein reconstituted with PLB4 taken from mother liquors used for protein crystallization. The Ca^{2+}-ATPase protein (12 µg) was added to 500 µl of buffer identical to that indicated above for determination of Ca^{2+}-ATPase activity with omission of NaN_3. Cross-linking was conducted with 1 mM KMUS for 2 min at room temperature. Reactions were stopped with 7.5 µl of gel loading buffer containing 15% SDS and 100 mM dithiothreitol. Samples were subjected to SDS-PAGE and immunoblotting with the anti-PLB antibody, 2D12, for detection of PLB cross-linked to SERCA1a (skeletal muscle isoform) (Fig. 3*C*). Cross-linking of the canine cardiac isoform of the Ca^{2+} pump (SERCA2a) to N30C-PLB or PLB4 co-expressed in insect cells was conducted identically as previously described (10) in 50 mM MOPS (pH 7.0), 100 mM KCl, and 1 mM Ca^{2+}: EGTA buffer in the presence or absence of 3 mM $MgCl_2$ (Fig. 6). Cross-linking was conducted with 1 mM KMUS for one minute at room temperature. The results shown in Fig. 6 were conducted in the absence of ATP, however, similar results were obtained with inclusion of 3 mM ATP. K_i values indicate Ca^{2+} concentrations at which cross-linking is inhibited by 50%.

RESULTS AND DISCUSSION

Crystallization of the PLB/SERCA Complex—Crystallizing the novel Ca^{2+}-free state of SERCA that binds PLB required that the solubilized enzyme be reconstituted with PLB in

the absence of Ca^{2+} (presence of EGTA). However, the Ca^{2+}-ATPase is extremely labile and prone to denaturation when solubilized without Ca^{2+} (24, 25), and the detergents typically used for SERCA solubilization/crystallization ($C_{12}E_8$) (15, 18, 26) and for PLB reconstitution with SERCA ($C_{12}E_8$ or octyl glucoside) (14, 27) had strong detrimental effects on Ca^{2+} affinity (Fig. 2*A*) and/or stability of the enzyme over time (Fig. 2*B*). For example, solubilizing SERCA in the absence of Ca^{2+} in $C_{12}E_8$ caused a 3-fold decrease in Ca^{2+} affinity and loss of enzyme activity with a $t_{1/2}$ of ~3 days at 4°C. Octyl glucoside, on the other hand, did not affect Ca^{2+} affinity, but caused even more rapid denaturation of the enzyme, with a $t_{1/2}$ of less than one day at 4°C.

Consequently, a major challenge was to develop a new detergent system that would facilitate co-crystallization of SERCA reconstituted with PLB without denaturing the enzyme. The nonionic detergent nonyl maltoside was ultimately selected for solubilization of SERCA as it had little effect on the Ca^{2+} affinity of the enzyme (K_{Ca} = 0.25 μM versus 0.21 μM in the absence of detergent) (Fig. 2*A*), and preserved 90-100% of the solubilized Ca^{2+}-ATPase activity for several weeks at 4°C (Fig. 2*B*). SERCA solubilized in nonyl maltoside was then reconstituted with WT-PLB or PLB4 solubilized in decyl maltoside or dodecyl maltoside (shown with PLB4 solubilized in decyl maltoside in Fig. 2*B*), detergents which also preserved SERCA catalytic activity for weeks at when stored at 4°C. Ca^{2+}-ATPase assays in the newly developed detergent system show that WT-PLB and PLB4 decreased the Ca^{2+} affinity of the solubilized enzyme by 2- and 5-fold, respectively, but had no significant effect on maximal ATPase activity measured at saturating Ca^{2+} concentrations (Fig. 3*B*). This alteration in the apparent Ca^{2+} affinity of SERCA is the hallmark of PLB inhibition (2, 3). As expected, addition of the 2D12 anti-PLB antibody (which mimics the effect of Ser^{16}/Thr^{17} phosphorylation of PLB (23)) largely reversed SERCA inhibition by WT-PLB and PLB4 (*shaded dotted lines*).

Ca^{2+}-dependent binding interactions between solubilized SERCA and PLB4 were also confirmed using chemical cross-linking. Cross-linking of residue N30C of PLB4 to Lys^{328} of SERCA with the heterobifunctional cross-linker KMUS (7, 10) was inhibited over the same Ca^{2+} concentration range (K_i = 1.6 μM) (Fig. 3*C*) as enzyme activation occurred (K_{Ca} = 1.4 μM) (Fig. 3*B*). This strongly suggests that PLB decreases the Ca^{2+} affinity of SERCA by disrupting Ca^{2+} binding (10) to the enzyme. Fig. 3 further confirms that normal protein-binding interactions between PLB and SERCA were maintained in the newly developed detergent system, recapitulating results previously observed with intact SR vesicles (16) or with ER membranes co-expressing the recombinant proteins (10). The remarkable stability of Ca^{2+}-free SERCA solubilized in nonyl maltoside is reported here for the first time.

It should be mentioned that rabbit skeletal muscle SR vesicles were used as the source of the Ca^{2+} pumps in this study due to the high content of the ATPase protein in the SR membrane, making enzyme purification unnecessary (15) (Fig. 3*D*). (SERCA1a is highly homologous to the cardiac isoform, SERCA2a, and is regulated identically by PLB (6). In addition, both WT-PLB and PLB4 prepared in alkyl mannosides were predominantly multimeric on SDS gels; WT-PLB was mostly pentameric, and PLB4 ran mostly as pentamers and tetramers. Boiling in 6% SDS prior to PAGE was required to destabilize these highly oligomeric forms of PLB (Fig. 3*D*), as observed previously with PLB purified in other detergents (14, 28).

Crystallization trials with SERCA solubilized in nonyl mannoside were conducted at pH 7.0 in the presence and absence of PLB4, nucleotides (ADP and ATP), and Ca^{2+}. In the absence of Ca^{2+} (1 mM EGTA), SERCA crystals grew only in the presence of PLB4, and crystal growth was inhibited by increasing Ca^{2+} concentration, consistent with PLB stabilizing a Ca^{2+}-free state of enzyme (5). Addition of ADP or ATP to the mother liquors appeared to improve crystal quality in some trials; however, no electron density corresponding to nucleotide bound to SERCA was resolved in any of these crystal forms (data not shown). Crystallization trials were also conducted with WT-PLB, but the naturally occurring protein proved inferior to PLB4 in promoting SERCA crystal growth, presumably because its lower affinity for SERCA relative to PLB4 (10) makes it less efficient at stabilizing the pump for crystallization.

PLB Binding Site on SERCA—The structure of *E*2-PLB at 2.83 Å resolution (Table 1)

shows PLB4 as an α-helix bound within a groove formed between transmembrane helices M2, M4, M6, and M9 of SERCA (Fig. 3*A*, *magenta helix*). Electron density corresponding to residues 21 to 49 of the 52 amino acids comprising PLB (Fig. 1) was observed. The α-helix extends uninterrupted from residue 21 in the cytoplasm to residue 49 in transmembrane domain. The N-terminal twenty residues of PLB, which includes residues Ser^{16} and Thr^{17} that are subject to phosphorylation, are not visible in the electron density, but were nonetheless functional in the mother liquors as evidenced by the effects of the 2D12 antibody (Fig. 3*B*). (Western blots of the re-solubilized crystals demonstrated that the PLB in *E*2-PLB was completely intact; PLB was detected at the appropriate mobility by the 2D12 antibody, which recognizes residues 7-14 of PLB, and by the 1F1 antibody, which recognizes residues 1-5 of PLB). Residues 50-52 of PLB, predicted previously to remain alpha helical (9), were also unobserved in the electron density. Consequently, it would appear that the central 29 residues of PLB form the majority of the stable inhibitory interactions with the Ca^{2+}-ATPase. The *E*2-PLB structure confirms the location of the PLB binding site on the cardiac enzyme (SERCA2a) predicted previously by chemical cross-linking (5, 7-9). The distances between specific amino acid residues of PLB and SERCA observed in the *E*2-PLB structure were expected to be consistent with the distances estimated by cross-linking (5-9, 16); however, we were surprised by how closely the experimental values agreed with those determined from the structure (Table 2), highlighting the utility of cross-linkers as molecular rulers.

PLB Effects on the Ca^{2+} Binding Sites— The signature effect of PLB is its ability to decrease the apparent Ca^{2+} affinity of SERCA, and the physical basis for this functional effect is now revealed in the *E*2-PLB structure. The two high affinity Ca^{2+}-binding sites (sites I and II) of SERCA, which are formed between transmembrane helices M4, M5, M6, and M8 near the cytoplasmic membrane interface (26), are both severely disrupted by PLB4 binding. Fig. 4*A* shows significant unraveling of the "M4 kink" induced by PLB4, and the side chain of the Ca^{2+} gating residue, Glu^{309}, now faces away from the Ca^{2+} binding sites (Fig. 4*B*). The three main chain carbonyls on M4 contributing to site II are also displaced, making site II non-existent in our structure. Site I is largely collapsed and would not support coordination of either Ca^{2+} or Mg^{2+} in the conformation induced by PLB4 binding (Fig. 4*B*). The contact of PLB4 with helices M4 and M6 appears to close site I for metal occupancy because the side chains of Asn^{768}, Glu^{771}, Asn^{796} and Asp^{800} are all too close to accommodate the binding of a metal ion between their side chains and the peptide carbonyl oxygen of Ala^{305}. In particular, the distance geometry of residues Asn^{768} and Asn^{796} suggests the orientation of their side chain amide groups are switched from the orientations compatible with metal ion coordination in order to support hydrogen bonding interactions with the peptide carbonyl oxygen of Ala^{305} and the side chain of Glu^{771} (Fig. 4*B*). Thus, with PLB4 bound to SERCA, the Ca^{2+} pump adopts a conformation that is incompatible with either Ca^{2+} or Mg^{2+} binding to sites I and II. The *E*2-PLB structure suggests that in order for the polar side chains and main chain carbonyls forming the Ca^{2+} binding sites to align properly, PLB4 must completely dissociate from its binding site in the groove between the M2, M4, M6, and M9. Conversely, close spacing of M2 and M9 in the Ca^{2+}-bound structure of SERCA (*E*1·Ca_2) (26) appears to be incompatible with PLB binding to the PLB binding site defined in our structure. This result confirms the cross-linking based theory of mutually exclusive binding of PLB and Ca^{2+} to SERCA (5-9), which has been controversial (29-31).

In the *E*2-PLB structure, Asn^{34} of PLB appears to be an important and highly organized region of contact specifically perturbing the Ca^{2+} binding sites (Fig. *5A)*. Asn^{34} forms critical contacts with the main chain carbonyl oxygen of Gly^{801} (M6) and with the side chains of Thr^{805} (M6) and Gln^{108} (M2) of SERCA. Gln^{108}, in turn, contacts the side-chain of Thr^{317}, which may influence the positioning of the important Ca^{2+}-site II ligand, Glu^{309} (5, 8). The highly structured network of contacts with Asn^{34} of PLB appears to initiate a repositioning of residues 795-804 within the M6 helix; Asn^{796} now interacts with carbonyl oxygen of Ala^{305} and Ca^{2+} binding site I is collapsed (Fig. 4*B*). These findings highlight the key role of Asn^{34} in the mechanism of PLB inhibition, and explain how the N34A mutation of PLB causes loss of PLB function (32), and how

the T795A, L802A, T805A, and F809A mutations in SERCA all partially attenuate PLB inhibition (33). Another SERCA mutation known to disable Ca^{2+} binding is G801V (34). Our structure provides a plausible explanation for this phenomenon since a side chain at position 801 would be impinged on by Val^{104} and reposition the M6 helix and its Ca^{2+} ligands, Asn^{796} and Glu^{800}, in a manner similar to how Asn^{34} repositions the M6 helix and these same Ca^{2+}-ligands to collapse the Ca^{2+} binding site upon PLB binding (Fig 5*A*).

Another functionally important residue of PLB, Leu^{31}, is located one turn of the α-helix above Asn^{34}, and only 3.7 Å away from Thr^{805} of SERCA. Leu^{31} fits in a hydrophobic pocket defined by the side chains of Leu^{802}, Ala^{806}, and Phe^{809} in M6, and Trp^{932} and Leu^{939} in M9 (Fig. 5, *A* and *B*). Like N34A, the L31A mutation completely disables PLB inhibition (32), whereas L31I preserves full functional activity (8). This suggests that hydrophobic interactions of the proper size between residue 31 of PLB and M6/M9 of SERCA are required for proper positioning of Asn^{34} and SERCA inhibition. The binding interface between PLB and SERCA is largely stabilized by hydrophobic interactions including Van der Waals contacts between carbon atoms (Fig. 5*B, grey*). The contact surface buries between 1100-1200 $Å^2$ and about 40% of the available surface area of PLB4 between residues 21-49. There are only a few polar contacts, specifically between the amide nitrogen of Asn^{34} (*blue*) and the main chain carbonyl of Gly^{801} and the amide carbonyl of Gln^{108} and side chain of Thr^{805} (all in *red*, Fig. 5*B*). It is particularly interesting that the extensive polar contacts surrounding Asn^{34} takes place in the context of a particularly hydrophobic surface, which likely enhances their impact on SERCA function.

Manipulation of side chain contacts between PLB and SERCA can enhance as well as attenuate PLB inhibitory function, explaining the superinhibitory nature of PLB4. For example, the N27A mutation (35) near the cytoplasmic membrane interface of PLB would allow PLB4 to bind more tightly to SERCA because the smaller side chain of Ala fits more snugly into the hydrophobic cleft between Phe^{809} (M6) and Trp^{932} (M9), where the distances between the methyl side chain of Ala and the two aromatic side chains are only 3.6-3.9 Å (Fig. 5*B*). Ala substitution at Leu^{37} in the bilayer interior (32, 36) is likewise expected to attenuate steric clash between the long alkyl side chain of Leu^{37} and the hydrophobic side chains of Ile^{103} and Val^{104} at M2 (Fig. 5*B*). The more compact side chain of Ile^{37} appears to fit the available space within this hydrophobic pocket better than Leu^{37}, which would also explain the superinhibitory effect of the L37I mutation (37). At the C-terminal end of PLB4 at the luminal membrane interface, residue 49 of PLB is very close to Val^{89} (M2) (Table 2) (6, 9). The smaller side chains of Ala or Gly at this position appears to reduce steric hindrance with Val^{89} (Fig. 5*B*), explaining the superinhibitory effects of the V49A and V49G mutations in PLB (9). Thus PLB4 inhibitory function is augmented by the additive effects of the N27A, L37A, and V49G mutations, each of which optimizes the packing interactions between PLB and hydrophobic residues in the Ca^{2+}-ATPase. This observation also explains why PLB4 binds to SERCA with an affinity greater than that of TG (10), which binds with sub-nanomolar affinity to the Ca^{2+} pump (11, 12).

It should be pointed out that the above interpretation of how the point mutations in PLB4 would alter PLB interactions with the Ca^{2+}-ATPase and enhance its inhibitory function are based upon the assumption that WT-PLB would stabilize the enzyme in a nearly identical state as that captured by PLB4. Indeed, the structure of SERCA with PLB4 bound suggests that the point mutations in PLB4 would have only localized structural affects relative to WT-PLB. Moreover, the distances between specific amino acids of PLB and SERCA determined by cross-linking are nearly identical, whether determined with PLB molecules of normal or superinhibitory strength, including cross-linking of WT-PLB in native human SR vesicles (16). The distances determined by cross-linking with the normal strength PLB mutants reported in Table 2 are in close agreement with the distances between the same residues observed in the PLB4/SERCA crystal structure. Therefore, the crystal structure of SERCA with WT-PLB bound is likely to be very similar to the PLB4 bound structure.

Multimeric Nature of PLB—PLB is a pentamer of identical monomers (28, 38, 39). It has been proposed for some time that there is a dynamic equilibrium between PLB pentamers and monomers in the SR membrane (40, 41), and that

the PLB monomer is responsible for binding to SERCA and inhibiting it (32, 36). Residues Leu^{37}, Ile^{40}, Leu^{44}, Ile^{47}, and Leu^{51} of PLB form the Leu/Ile zipper (40) that stabilizes the non-inhibitory PLB pentamer (41); Ala substitution at any of these residues promotes pentamer dissociation, an increase in PLB monomers, and increased enzyme inhibition (32, 36). It was also suggested that PLB has two distinct functional faces located on opposite sides of the transmembrane helix: the Leu/Ile zipper face which when PLB is bound to SERCA points away from the enzyme and is involved only in PLB pentamer formation, and the inhibitory face which comes in direct contact with the Ca^{2+}-ATPase and mediates enzyme inhibition (32). Here we find that this idea is indeed correct for the Ile arm of the zipper; the heptad repeat of Ile zipper residues 40 and 47 is oriented away from the Ca^{2+}-pump when the PLB monomer is bound to the enzyme (Figs. 4*A* and 5*C, magenta*). In contrast, on the Leu arm of the zipper, both Leu^{37} (mutated to Ala in PLB4) and Leu 44 make direct contact with the Ca^{2+} pump at M2 (at Ile^{103} and Val^{104}, and at Leu^{96}, respectively) (Figs. 4*A* and 5*B*), consistent with the dual role of these two zipper residues in both pentamer formation and enzyme inhibition (37). At other positions along the transmembrane helix of PLB, residues Phe^{35}, Ile^{38}, Cys^{41}, Leu^{42}, Ile^{45}, and Ile^{48} all make direct contact with non-polar residues in several transmembrane helices of SERCA (Fig. 5, *B* and *C*), contributing to the high binding affinity of the PLB monomer for the Ca^{2+}-ATPase (10,16).

It should be noted that the mobility forms of WT-PLB and PLB4 observed on SDS gels are quite different. Whereas WT-PLB ran predominately as pentamers with a small amount of monomers, all five mobility forms of PLB4 were observed (Fig. 3*D*). Prior to boiling in 6% SDS, pentamers and tetramers predominated with PLB4; after boiling in SDS, monomers and dimers were the main mobility forms. The significance of this observation became apparent when we discovered additional weak electron density embedded in the membrane near PLB4 in all of our datasets (Figs. 3*A*, 4*A*, 5*A*, and 5*C*, *yellow helices*). The electron density is consistent with a 14 amino acid-long α-helix (*yellow*) that is in direct contact with the outer face of the PLB4 monomer directly bound to SERCA (*magenta*), but this second helix does not contact SERCA. The nature of the observed electron density for this second helical region (PLB (chain C) in Table 1) indicates significant conformational freedom, low occupancy, or both. This density was able to accommodate the PLB4 sequence, but was not compatible with the sarcolipin (SLN) sequence register, and PLB4 dimers were also present in our re-solubilized crystals run on SDS-PAGE (data not shown). Therefore, the extra helix is most likely attributable to a second PLB4 molecule bound to PLB but not physically in contact with SERCA. Residues Phe^{32}, Cys^{36}, Leu^{39}, Ile^{40}, Leu^{43} and Ile^{47} of PLB4 appear to be interacting with residues Cys^{30}, Ile^{33}, Cys^{36}, Ala^{37}, and Ile^{40} of the second PLB4 molecule, which includes the two Ile zipper residues (40 and 47) that help to stabilize PLB pentamers (Figs. 4*A* and 5*C*).

Although PLB4 is largely pentameric or tetrameric when purified in non-denaturing detergents, the crystal structure clearly indicates that the PLB monomer forms the important contact surface between PLB4 and SERCA (Fig. 5*C*). No PLB4 pentamers or tetramers attached to SERCA were identified in any of the datasets. Therefore, a reversible equilibrium (32, 36) between pentamer-tetramers and monomer-dimers of PLB4 must exist in order to allow regulatable inhibition of SERCA activity over the range of Ca^{2+} concentrations depicted in Fig. 3, *B* and *C*. Consistent with this, at the molar ratio of PLB to SERCA used for crystal formation (2.9 to 1), there are sufficient dimers, but insufficient pentamers or tetramers, to allow complete inhibition of SERCA at the lower Ca^{2+} concentrations assayed (Fig. 3*B*). Pentamer formation by monomers released from SERCA thus appears to aid in complete reversal of enzyme inhibition at saturating Ca^{2+} concentration (Fig. 3, *A* and *C*), as recently demonstrated using intact SR vesicles from human hearts (16).

The structure is therefore consistent with there being an equilibrium between PLB/SERCA heterodimers, free PLB monomers, and PLB pentamers in the SR membrane, with reversible exchange of PLB protomers between the different oligomeric states. Even though PLB4 is strongly bound to the enzyme in the absence of Ca^{2+}, there is still a reversible equilibrium with PLB continuously associating and dissociating from SERCA. During this rapid exchange, the collapsed Ca^{2+} binding sites can briefly re-form,

providing an opportunity for a Ca^{2+} to bind to the enzyme. High Ca^{2+} concentrations shift the binding equilibrium towards PLB dissociation, which is aided by the fact that the free PLB molecules can oligomerize into stable homopentamers.

The Conformation of SERCA that Binds PLB—The structure of SERCA in the PLB4/SERCA complex is distinct from the previously determined structures of SERCA in the *E*2 (low Ca^{2+} affinity) or *E*1 (high Ca^{2+} affinity) state (26). The Ca^{2+}-ATPase in our structure is globally similar to *E*1·Ca_2 in the overall spacing of the transmembrane helices and in the open arrangement of the cytoplasmic headpiece (Fig. 3*A*). However, unlike *E*1·Ca_2, the M1 helix in the PLB4–bound Ca^{2+} pump structure is positioned lower in the membrane, and is distinctly bent at Leu^{60}. In this position, the "M1 sliding door" that controls the opening to the purported Ca^{2+} access channel is open, exposing a number of negatively charged residues that lead to the Ca^{2+} binding sties (26, 42). An open Ca^{2+} access channel, as observed in our structure, is a key feature of the enzyme in the *E*2 state (26, 42). In addition, the metal-free Ca^{2+} binding sites in the PLB4/SERCA complex more closely resemble *E*2 than *E*1 (24). PLB4 contacts with M4 and M6 appear to stabilize hydrogen bonding between residues Asn^{796}, Asn^{768}, Glu^{771}, and the main-chain carbonyl of Ala^{305} (Fig. 5*D*). Although the spatial arrangement is somewhat different, conceptually similar interactions are observed in the metal-free Ca^{2+} binding sites in the *E*2-TG structure (24 and Fig. 5*D*). The apparent hydrogen bonding at the Ca^{2+} binding sites is consistent with the enzyme being protonated; it is generally accepted that protons stabilize the empty Ca^{2+} binding sites in the *E*2 state (26, 42). Therefore, PLB stabilizes a structure in which the Ca^{2+} binding sites are collapsed and appear to be protonated, and we define this structure as *E*2-PLB.

While this manuscript was in preparation, two separate groups (Toyoshima *et al.* (43) and Winther *et al.* (44) published crystal structures of Ca^{2+}-free SERCA stabilized by very high concentrations of $MgSO_4$ (40-75 mM) (referred to hereafter as *E*1·Mg (43)). The structures were nearly identical, and both had sarcolipin (SLN) bound. SLN is a 31 amino acid, skeletal-muscle "homologue" of PLB with ambiguous function (Fig. 1). Since the contacts between SLN and SERCA observed in the *E*1·Mg structures were similar to PLB/SERCA interactions determined previously by cross-linking (5-9), both groups postulated that the *E*1·Mg state they crystallized is the same state that binds PLB. On a global scale, PLB and SLN appear to bind to similar conformations of the transmembrane domain of SERCA, albeit with distinct orientations of the cytoplasmic domains. However, at the molecular level, notable structural differences in their respective transmembrane domains support that PLB stabilizes a distinct conformation of SERCA. Specifically, the Ca^{2+} binding sites in the *E*1·Mg structures are partially formed and have a distinctly *E*1-like appearance. On the other hand, in the metal-free *E*2 state that binds PLB, the Ca^{2+} binding sites are completely collapsed with interactions more similar to *E*2 than *E*1. In contrast to claims in these two recent papers (43, 44), the effects of SLN on Ca^{2+}-ATPase activity are different from those of PLB and remain controversial—no effect, Ca^{2+} affinity effects, V_{max} effects, and uncoupling effects of SLN have all been reported (27, 45-47). In detailed comparative studies, two separate groups recently concluded that SLN and PLB regulate SERCA by completely different mechanisms (27, 45). In one study, SLN effects on Ca^{2+}-ATPase activity were attributed to the unique C-terminal tail of SLN (containing Arg^{27} and Tyr^{31}), which is not found in PLB (27). In the second study, SLN had no effect on Ca^{2+}-ATPase activity, but instead uncoupled Ca^{2+} transport from ATP hydrolysis, and SLN continued to interact with SERCA in the presence of Ca^{2+} (45), in contrast to PLB, which dissociates from SERCA in the presence of Ca^{2+} (5). Therefore, unlike the recent SLN-bound *E*1·Mg structures, the PLB induced structural changes in SERCA observed presently have clear mechanistic implications that are consistent with PLB effects on Ca^{2+}-affinity (2).

The physiological significance of the *E*1·Mg state of SERCA is also worth discussion. In both studies mentioned above (43, 44), the structures were solved with the Ca^{2+}-free enzyme solubilized in $C_{12}E_8$, a condition known to cause irreversible enzyme inactivation (24, 25) (Fig. 2). It seems likely that at the high concentrations of $MgSO_4$ utilized, Mg^{2+} was acting as a surrogate for Ca^{2+}, thereby preventing enzyme denaturation.

However, whether the *E*1·Mg state occurs at physiological Mg^{2+} concentration is unknown, and the functional role of the putative state is unclear. Toyoshima *et al.* (43) concluded that *E*1·Mg is an obligate intermediate in the catalytic cycle of SERCA and that Mg^{2+} binding accelerates Ca^{2+} binding by reducing the energy required for formation of *E*1·Ca. On the other hand, Winther *et al.* (44) concluded the opposite, that Mg^{2+} binding to the "low affinity Mg^{2+} sites" actually retards SERCA activation by Ca^{2+}.

Cross-linking of PLB to SERCA can be used to test whether Mg^{2+} is required for PLB binding, and whether Mg^{2+} affects SERCA Ca^{2+} affinity, as postulated by Toyoshima *et al.* (43) and Winther *et al.* (44). Using both N30C-PLB, which alters Ca^{2+} affinity like WT-PLB, and PLB4, which supershifts Ca^{2+} affinity, we found that physiological concentrations of Mg^{2+} (3 mM) had no effect on the extent of PLB cross-linking to SERCA, and only minor effects on K_i values for Ca^{2+} inhibition of PLB cross-linking, thus reflecting minimal effects of Mg^{2+} on Ca^{2+} affinity of the enzyme (Fig. 6). Clearly, *E*1·Mg is not the state required for PLB binding, as was recently proposed (45, 46). Moreover, based upon our crystal structure and cross-linking results (Fig. 6), we conclude that the *E*1·Mg state of SERCA obtained at 40-75 mM $MgSO_4$ (45, 46) does not exist at physiological Mg^{2+} concentration (~ 3 mM).

In conclusion, we have determined the crystal structure of PLB4 bound to a unique metal-free *E*2 state of SERCA, one of the critical outstanding conformational states of the Ca^{2+}-ATPase remaining to be solved (5, 10). Interpreted in light of the extensive biochemical and physiological studies on PLB (2, 3), the new SERCA structure has allowed us to explain how through direct effects on Ca^{2+} affinity, dephosphorylated PLB inhibits SERCA activity and decreases contractility of the heart. Co-crystallization of PLB4 with SERCA was achieved using a newly developed detergent system specifically designed to maintain SERCA catalytic activity and normal regulation by PLB after solubilization in the absence of Ca^{2+}. Using this new system, it should be possible to crystallize SERCA with other forms of PLB, including WT-PLB, and ultimately to resolve the binding site for the N-terminus of PLB on the Ca^{2+} pump, which has remained problematical (6, 7, 48). The N-terminal domain of PLB is of particular physiological interest because β-adrenergic-receptor stimulated phosphorylation of PLB at Ser^{16} and Thr^{17} is fundamental to the mechanism by which PLB regulates myocardial contractility (1, 4).

REFERENCES

1. Lindemann, J.P., Jones, L.R., Hathaway, D.R., Henry, B.G., and Watanabe, A. M. (1983) β-adrenergic stimulation of phospholamban phosphorylation and Ca^{2+}-ATPase activity in guinea pig ventricles. *J. Biol. Chem.* **258**, 464-471
2. Simmerman, H.K., and Jones, L.R. (1998) Phospholamban: protein structure, mechanism of action, and role in cardiac function. *Physiol. Rev.* **78**, 921–947
3. Young, H.S., and Stokes, D.L. (2004) The mechanics of calcium transport. *J. Membr. Biol.* **198**, 55-63
4. Wegener, A.D., Lindemann, J.P., Simmerman, H.K.B., and Jones, L.R. (1989) Phospholamban phosphorylation in intact ventricles: Phosphorylation of serine 16 and threonine 17 in response to β-adrenergic stimulation. *J. Biol. Chem.* **264**, 11468-11474
5. Jones, L.R., Cornea, R.L., and Chen, Z. (2002) Close proximity between residue 30 of phospholamban and cysteine 318 of the cardiac Ca^{2+} pump revealed by intermolecular thiol cross-linking. *J. Biol. Chem.* **277**, 28319-28329
6. Toyoshima, C., Asahi, M., Sugita, Y., Khanna, R., Tsuda, T., and MacLennan, D.H. (2003) Modeling of the inhibitory interaction of phospholamban with the Ca^{2+} ATPase. *Proc. Natl. Acad. Sci. USA* **100**, 467-472
7. Chen, Z., Stokes, D.L., Rice, W.J., and Jones, L.R. (2003) Spatial and dynamic interactions between phospholamban and the canine cardiac Ca^{2+} pump revealed with use of heterobifunctional cross-linking agents. *J. Biol. Chem.* **278**, 48348-48356

8. Chen, Z., Stokes, D.L., and Jones, L.R. (2005) Role of leucine 31 of phospholamban in structural and functional interactions with the Ca^{2+} pump of cardiac sarcoplasmic reticulum. *J. Biol. Chem.* **280**, 10530-10539
9. Chen, Z., Akin, B.L., Stokes, D.L., and Jones, L.R. (2006) Cross-linking of C-terminal residues of phospholamban to the Ca^{2+} pump of cardiac sarcoplasmic reticulum to probe spatial and functional interactions within the transmembrane domain. *J. Biol. Chem.* **281**, 14163-14172
10. Akin, B.L., Chen, Z., and Jones, L.R. (2010) Superinhibitory phospholamban mutants compete with Ca^{2+} for binding to SERCA2a by stabilizing a unique nucleotide-dependent conformational state. *J. Biol. Chem*. **285**, 28540-28552
11. Lytton, J., Westlin, M., and Hanley, M. R. (1991) Thapsigargin inhibits the sarcoplasmic or endoplasmic reticulum Ca-ATPase family of calcium pumps. *J. Biol. Chem.* **266**, 17067–17071
12. Sagara, Y., Fernandez-Belda, F., de Meis, L., and Inesi, G. (1992) Characterization of the inhibition of intracellular Ca^{2+} transport ATPases by thapsigargin. *J. Biol. Chem.* **267**, 12606–12613
13. Jones, L.R., Besch, H.R., Jr, and Watanabe, A.M. (1978) Regulation of the calcium pump of cardiac sarcoplasmic reticulum. Interactive roles of potassium and ATP on the phosphoprotein intermediate of the (K^+,Ca^{2+})-ATPase. *J. Biol. Chem.* **253**, 1643-1653
14. Reddy, L.G., Jones, L.R., Cala, S.E., O'Brian, J.J., Tatulian, S.A., and Stokes, D.L. (1995) Functional reconstitution of recombinant phospholamban with rabbit skeletal Ca^{2+}-ATPase. *J. Biol. Chem.* **270**, 9390-9397
15. Sørensen, T.L., Olesen, C., Jensen, A.M., Møller, J.V., and Nissen, P. (2006) Crystals of sarcoplasmic reticulum Ca^{2+}-ATPase. *J. Biotechnol.* **124**, 704-716
16. Akin, B.L., and Jones, L. R. (2012) Characterizing phospholamban to sarco(endo)plasmic reticulum Ca^{2+}-ATPase 2a (SERCA2a) protein binding interactions in human cardiac sarcoplasmic reticulum vesicles using chemical cross-linking. *J. Biol. Chem*. **287**, 7582-7593
17. Otwinowski, Z., and Minor, W. (1997) Processing of X-ray diffraction data collected in oscillation mode. *Methods Enzymol.* **276**, 307-326
18. Jensen, A.M., Sørensen, T. L., Olesen, C., Møller, J. V., and Nissen, P. (2006) Modulatory and catalytic modes of ATP binding by the calcium pump. *EMBO J.* **25**, 2305–2314
19. McCoy, A.J., Grosse-Kunstleve, R.W., Adams, P.D., Winn, M.D., Storoni, L.C., and Read, R.J. (2007) Phaser crystallographic software. *J. Appl. Cryst.* **40**, 658-674
20. Emsley, P., Lohkamp, B., Scott, W.G., and Cowtan, K. (2010) Features and development of Coot. *Acta Crystallographica. Section D, Biological Crystallography* **66(Pt 4)**, 486-501
21. Murshudov, G.N., Vagin, A.A., and Dodson, E.J. (1997) Refinement of macromolecular structures by the maximum-likelihood method. *Acta Crystallographica. Section D, Biological Crystallography* **53 (Pt 3)**, 240-250
22. Painter, J., and Merritt, E.A. (2006) Optimal description of a protein structure in terms of multiple groups undergoing TLS motion. *Acta Crystallographica. Section D, Biological Crystallography* **62(Pt 4)**, 439-450
23. Chen, Z., Akin, B.L., and Jones, L.R. (2007) Mechanism of reversal of phospholamban inhibition of the cardiac Ca^{2+}-ATPase by protein kinase A and by anti-phospholamban monoclonal antibody 2D12. *J. Biol. Chem.* **282**, 20968-20676
24. Toyoshima, C., and Nomura, H. (2002) Structural changes in the calcium pump accompanying the dissociation of calcium. *Nature* **418**, 605-611
25. Montigny C., Arnou, B., and Champeil, P. (2010) Glycyl betaine is effective in slowing down the irreversible denaturation of a detergent-solubilized membrane protein, sarcoplasmic reticulum Ca^{2+}-ATPase (SERCA1a). *Biochem. Biophys. Res. Commun.* **391**, 1067-1069
26. Toyoshima, C. (2008) Structural aspects of ion pumping by Ca^{2+}-ATPase of sarcoplasmic reticulum. *Arch. Biochem. Biophys.* **476**, 3–11

27. Gorski, P.A., Glaves, J.P., Vangheluwe, P., and Young, H.S. (2013) Sarco(endo)plasmic reticulum calcium ATPase (SERCA) inhibition by sarcolipin is encoded in its luminal tail. *J. Biol. Chem.* **288**, 8456-8467
28. Jones, L.R., Simmerman, H.K., Wilson, W.W., Gurd, F.R., and Wegener, A.D. (1985) Purification and characterization of phospholamban from canine cardiac sarcoplasmic reticulum. *J. Biol. Chem.* **260**, 7721-7730
29. Mueller, B., Karim, C.B., Negrashov, I.V., Kutchai, H., and Thomas, D.D. (2004) Direct detection of phospholamban and sarcoplasmic reticulum Ca-ATPase interaction in membranes using florescence resonance energy transfer. *Biochemistry* **43**, 8754-8765
30. Li, J., Bigelow, D.J., and Squier, T.C. (2004) Conformational changes within the cytoplasmic portion of phospholamban upon release of Ca-ATPase inhibition. *Biochemistry.* **43**, 3870-3879
31. Bidwell, P., Blackwell, D.J., Hou, Z., Zima, A.V., and Robia, S.L. (2011) Phospholamban binds with differential affinity to calcium pump conformers. *J. Biol. Chem.* **286**, 35044-35050
32. Kimura, Y., Kurzydlowski, K., Tada, M., and MacLennan, D.H. (1997) Phospholamban inhibitory function is activated by depolymerization. *J. Biol. Chem.* **272**, 15061-15064
33. Asahi, M., Kimura, Y., Kurzydlowski, K., Tada, M., and MacLennan, D. H. (1999) Transmembrane helix M6 in sarco(endo)plasmic reticulum Ca^{2+}-ATPase forms a functional interaction site with phospholamban. Evidence for physical interactions at other sites. *J. Biol. Chem.* **274**, 32855–32862
34. Andersen, J.P, Vilsen, B., and MacLennan, D.H. (1992) Functional consequences of alterations to Gly310, Gly770, and Gly801 located in the transmembrane domain of the Ca^{2+}-ATPase of sarcoplasmic reticulum. *J. Biol. Chem.* **267**, 2767-2774
35. Kimura, Y., Asahi, M., Kurzydlowski, K., Tada, M., and MacLennan, D.H. (1998) Phospholamban domain Ib mutations influence functional interactions with the Ca^{2+}-ATPase isoform of cardiac sarcoplasmic reticulum. *J. Biol. Chem.* **273**, 14238-14241
36. Autry, J.M., and Jones, L.R. (1997) Functional co-expression of the canine cardiac Ca^{2+} pump and phospholamban in *Spodoptera frugiperda* (Sf21) cells reveals new insights on ATPase regulation. *J. Biol. Chem.* **272**, 15872-15880
37. Cornea, R.L., Autry, J.M., Chen, Z., and Jones, L.R. (2000) Reexamination of the role of the leucine/isoleucine zipper residues of phospholamban in inhibition of the Ca^{2+} pump of cardiac sarcoplasmic reticulum. *J. Biol. Chem.* **275**, 41487-41494
38. Wegener, A.D., and Jones, L.R. (1984) Phosphorylation-induced mobility shift in phospholamban in sodium dodecyl sulfate-polyacrylamide gels. Evidence for a protein structure consisting of multiple identical phosphorylatable subunits. *J. Biol. Chem*. **259**,1834-1841
39. Simmerman, H.K., Collins, J.H., Theibert, J.L., Wegener, A.D., and Jones, L.R. (1986) Sequence analysis of phospholamban. Identification of phosphorylation sites and two major structural domains. *J. Biol. Chem.* **261**, 13333-13341
40. Simmerman, H.K., Kobayashi, Y.M., Autry, J.M., and Jones, L.R. (1996) A leucine zipper stabilizes the pentameric membrane domain of phospholamban and forms a coiled-coil pore structure. *J. Biol. Chem.* **271**, 5941-5946
41. Cornea, R.L., Jones, L.R., Autry, J.M., and Thomas, D.D. (1997) Mutation and phosphorylation change the oligomeric structure of phospholamban in lipid bilayers. *Biochemistry* **36**, 2960-2967
42. Bublitz, M., Musgaard. M., Poulsen, H., Thøgersen, L., Olesen, C., Schiøtt, B., Morth, J.P., Møller, J.V., and Nissen, P. (2013) Ion pathways in the sarcoplasmic reticulum Ca^{2+}-ATPase. *J. Biol. Chem.* **288**, 10759-10765
43. Toyoshima, C., Iwasawa, S., Ogawa, H., Hirata, A., Tsueda, J., and Inesi, G. (2013) Crystal structures of the calcium pump and sarcolipin in the Mg^{2+}-bound E1 state. *Nature* **495**, 260-264
44. Winther, A.M., Bublitz, M., Karlsen, J.L., Møller, J.V., Hansen, J.B., Nissen, P., and Buch-Pedersen, M.J. (2013) The sarcolipin-bound calcium pump stabilizes calcium sites exposed to the cytoplasm. *Nature* **495**, 265-269
45. Sahoo, S.K., Shaikh, S.A., Sopariwala, D.H., Bal, N.C., and Periasamy, M. (2013) Sarcolipin

protein interaction with sarco(endo)plasmic reticulum Ca^{2+} ATPase (SERCA) is distinct from phospholamban protein, and only sarcolipin can promote uncoupling of the SERCA pump. *J. Biol. Chem.* **288**, 6881-6889

46. Odermatt, A., Becker, S., Khanna, V.K., Kurzydlowski, K., Leisner, E., Pette, D., and MacLennan, D.H. (1998) Sarcolipin regulates the activity of SERCA1, the fast-twitch skeletal muscle sarcoplasmic reticulum Ca^{2+}-ATPase. *J. Biol. Chem.* **273**, 12360-12369
47. Lytton, J., Westlin, M., Burk, S.E., Shull, G.E., and MacLennan, D.H. (1992) Functional comparisons between isoforms of the sarcoplasmic or endoplasmic reticulum family of calcium pumps. *J. Biol. Chem.* **267**, 14483-11489
48. James, P., Inui, M., Tada, M., Chiesi, M., and Carafoli, E. (1989) Nature and site of phospholamban regulation of the Ca^{2+} pump of sarcoplasmic reticulum. *Nature* **342**, 90-92

Acknowledgements—We thank the staff at Beamline 9-ID at the Advanced Photon Source within Argonne National Laboratory and we thank Glen Schmeisser for excellent technical assistance.

FOOTNOTES

*This work was supported by NIH grants R37-HL049428 (L.R.J), and R01-AA18123 and R01-DK79887 (T.D.H).

[1]To whom correspondence should be addressed: Krannert Institute of Cardiology, 1800 N. Capitol Ave., Indianapolis, IN, 46202 Tel.: 317-274-0961 Fax: 317-962-0505 E-mail: bbudryns@iu.edu

[2]To whom correspondence should be addressed: Krannert Institute of Cardiology, 1800 N. Capitol Ave., Indianapolis, IN, 46202 Tel.: 317-962-0960 Fax: 317-962-0505 E-mail: lrjones@iu.edu

[3]The abbreviations used are: SR, sarcoplasmic reticulum; PLB, phospholamban; SERCA, sarco(endo)plasmic reticulum Ca^{2+}-ATPase; SERCA1a, fast skeletal muscle isoform of SERCA; SERCA2a, cardiac isoform of SERCA; WT-PLB, wild-type PLB; PLB4, N27A, N30C, L37A, V49G-PLB; 2D12, anti-PLB monoclonal antibody; M, transmembrane domain; *E*1, high Ca^{2+}-affinity conformation of Ca^{2+}-ATPase; *E*2, low Ca^{2+} affinity conformation of Ca^{2+}-ATPase; MOPS, 3-(N-morpholino)propanesulfonic acid; decyl maltoside, n-decyl-β-D-maltopyranoside; nonyl maltoside, n-nonyl-β-D-maltopyranoside; dodecyl maltoside, n-dodecyl-β-D-maltopyranoside; $C_{12}E_8$, octaethylene glycol monododecyl ether; octyl glucoside, octyl β-D-glucopyranoside; K_{Ca}, Ca^{2+} concentration required for half-maximal effect; K_i, Ca^{2+} concentration giving half-maximal inhibition; KMUS, N-kappa-Maleimidoundecanoyl-oxysulfosuccinimide ester; SLN, sarcolipin

Table 1. Data collection and refinement statistics

	SERCA/PLB4
Data Collection	
Space group	$P2_12_12_1$
Cell dimensions	
a, b, c (Å)	61.59, 93.09, 316.4
Cell angles (a, b, g °)	90.0, 90.0, 90.0
Resolution (Å)	50.0-2.83 (2.89-2.83)
R_{merge}(%)	8.4 (49.2)
$I / s_{<I>}$	13.2 (2.0)
Completeness (%)	97 (97)
Redundancy	5.5 (4.5)
Wilson B-value ($Å^2$)	88.5
Refinement	
Resolution (Å)	50.0-2.83
No. reflections	42925
R_{work} / R_{free}(%)	23.9/28.4
No of atoms	
Protein	7861
Ligand/ion	47
B-factors ($Å^2$)	
Serca (chain A)	89.6
PLB (chain B)	140.2
PLB (chain C)	183.4
Ligand/ion	85.5
R.m.s deviations	
Bond lengths (Å)	0.009
Bond angles (°)	1.20
Ramachandran Plot	
Core	88.9
Allowed	11.0

Table 2. Distances between residues of PLB and SERCA determined by cross-linking (X-link) versus x-ray diffraction (Crystal)

		Distance (Å)		
PLB	SERCA	X-link	Crystal	Ref.
N27C	K328	9–14	14	7
*K27	K328	8	10-13	16
N30C	C318	10	10	5
N30C	K328	14–16	17	7
L31C	T317C	10	10	8
V49C	V89C	0–5	5	6,9
M50C	V89C	10	ND	9
L52C	V89C	5	ND	9

Cross-linking distances between residues of PLB and SERCA were determined after co-expression of selected mutants of PLB with SERCA2a (5, 7-9) or SERCA1a (6) in microsomal membranes, or with native PLB and SERCA2a in human cardiac SR vesicles (16). Cross-linking was conducted with homo- or heterobifunctional cross-linking reagents (5, 7-9, 16) or with copper phenanthrolene (6). The distances in the PLB4/SERCA crystal structure were determined by measuring from the β-carbon of the PLB residue to the closest side chain atom of the corresponding SERCA residue (native protein). For V49G in PLB4 the distance was measured from the α-carbon of Gly^{49}. ND, not determinable. *The distance measurement between K27 and K328 was estimated by computational mutation of A27 to K and selecting side chain rotomers compatible with the local structure for both K27 and K328, then measuring the closest approaches for the side chains.

FIGURE LEGENDS

FIGURE 1. **Amino acid sequences of PLB4 and WT-PLB (canine isoforms), and rabbit SLN**. Cytoplasmic and transmembrane domains are shown as well as the phosphorylated residues Ser^{16} and Thr^{17} of PLB. Mutations in PLB4 are shaded in blue. Amino acid residues common to both PLB and SLN are shaded in yellow.

FIGURE 2. **Effect of detergent solubilization of SERCA on apparent Ca^{2+} affinity (*A*) and Ca^{2+}-ATPase stability over time (*B*).** Mother liquors were prepared from rabbit skeletal SR vesicles in buffer containing 2% detergent concentrations and 2 mM EGTA as described under EXPERIMENTAL PROCEDURES. *A*, apparent Ca^{2+} affinity (K_{Ca}) of the solubilized Ca^{2+}-ATPase was determined immediately after membrane solubilization by measuring Ca^{2+} activation of ATP hydrolysis. Results are expressed as percentage of the maximal Ca^{2+}-ATPase activity obtained for each detergent tested: NM (nonyl glucoside), OG (octyl glucoside), DM (decyl maltoside), DDM (dodecyl maltoside). Control membranes (Con) were not treated with detergent. K_{Ca} values (μM) were 0.21 ± 0.005 (Con), 0.25 ± 0.02 (NM), 0.23 ± 0.02 (OG), 0.63 ± 0.02 ($C_{12}E_8$), 0.29 ± 0.01 (DM), and 0.40 ± 0.02 (DDM). Mean ± S. E. from 4 - 8 determinations. *B*, enzyme stability of SERCA was monitored after storage of the mother liquors in different detergents at 4 °C for the times indicated. At the designated times of storage, aliquots were taken for assay of Ca^{2+}-ATPase activity (μmol P_i/mg protein/h) at saturating Ca^{2+} concentration (50 μM Ca^{2+}). NM + PLB4 designates SERCA solubilized in NM reconstituted with PLB in DM, an optimal condition for crystal formation. Shown is one representative experiment, which was repeated at least three times for all the different detergents with similar results.

FIGURE 3. **Crystal structure and functional characterization of the PLB4/SERCA complex.** *A*, a ribbon model of the complex between SERCA and PLB4. In SERCA the cytoplasmic headpiece consists of actuator (A) (*grey*), phosphorylation (P) (*gold*), and nucleotide-binding (N) (*green*) domains. The transmembrane domain helices of SERCA are colored *cyan*, except for M4, which is colored *blue*. The bound PLB4 molecules are colored *magenta* (chain B) and *yellow* (chain C) (Table 1). The figure was generated using PyMOL (The PyMOL Molecular Graphics System, Version 1.5.0.4 Schrödinger, LLC.). *B*, Ca^{2+}-ATPase activity of nonyl maltoside-solubilized SERCA alone and after reconstitution with purified, solubilized WT-PLB or PLB4. Activity was measured in the presence and absence of the anti-PLB monoclonal antibody, 2D12. K_{Ca} values (μM) for Ca^{2+} activation of ATP hydrolysis were: No PLB, 0.26 ± 0.01; WT-PLB, 0.62 ± 0.03, and 0.35 ± 0.02 (+ 2D12); PLB4, 1.38 ± 0.07, and 0.53 ± 0.03 (+ 2D12). Means ± S. E. from 3-6 determinations. *C*, anti-PLB immunoblot showing Ca^{2+} effect on cross-linking of PLB4 to SERCA with KMUS under the same conditions used for determination of Ca^{2+}-ATPase activity. K_i value (μM) for Ca^{2+} inhibition of cross-linking was 1.60 ± 0.16. Mean ± S. E. from 6 determinations. *D*, coomassie-blue stained gel showing SERCA solubilized from rabbit skeletal muscle SR membranes and WT-PLB and PLB4 purified in decyl maltoside (± boil). 10 μg of membrane protein were electrophoresed per gel lane.

FIGURE 4. **Binding of PLB4 to the transmembrane domain of SERCA**. *A*, a view of PLB4 bound to SERCA roughly orthogonal to that in Figure 3*A* including the side chains of PLB4 interacting with the transmembrane domain; color scheme is identical to Figure 3*A*. *B*, a horizontal section of the SERCA

transmembrane domain showing the interaction area of PLB4 in the proximity of the Ca^{2+}-binding sites – color scheme is identical to Figure 3*A*. Critical side chains are labeled and displayed, as are the nearby transmembrane helices. The dotted lines and numerical values indicate the distances between potential hydrogen bond donors and acceptors. Figure generated using PyMOL.

FIGURE 5. **Critical interactions at the interface between SERCA and PLB4.** *A*, a horizontal section of the SERCA transmembrane domain centered near the key inhibitory residue Asn^{34} of PLB4. The color scheme is identical to Fig. 4*A*. Key residues at the interaction surface are labeled, as are the individual transmembrane helices in this region. The dotted line indicates inferred hydrogen bonding between donor and acceptor atoms and the numerical value indicates the distance between atoms potentially sharing hydrogens. *B*, a "peeled" surface view of the interaction surface between PLB4 and SERCA. For this figure, PLB4 was rotated 180 degrees in the vertical plane and translated to the right hand side of this figure in order to expose the interacting surfaces and their chemical character. The color scheme utilizes "atom-type" coloring (*blue* for nitrogen, *red* for oxygen, *yellow* for sulfur and *green* for carbon atoms not involved in the contact surface between PLB4 and SERCA). Carbon atoms in amino acids residing either in PLB4 or in SERCA that have at least one atom at the contact surface are colored *grey*. Amino acid residues that form the contact surface are labeled. *C*, the original figure-of-merit sA-weighted 2Fo-Fc (*blue*) and Fo-Fc (*green*) electron density maps for PLB4 bound to the transmembrane domain of SERCA generated prior to their inclusion in the model, superimposed on the final refined coordinates for the complex. *D*, structural super-positioning of the PLB4/SERCA complex (*cyan* and *magenta* ribbons for SERCA and PLB4) with that of the Ca^{2+}-free *E*2 complex stabilized by TG (*green* ribbons, RCSB code 1IWO (24)). The structures were super-imposed utilizing the C-alpha atoms of residues 750-990. Key residues involved in Ca^{2+}-binding are labeled, as is Ile^{38} of PLB4.

FIGURE 6. **Lack of effect of Mg^{2+} on PLB cross-linking.** *A*, autoradiograph showing cross-linking of N30C-PLB or PLB4 to SERCA2a expressed in insect cell membranes. Cross-linking was conducted with KMUS over a range of Ca^{2+} concentrations in the presence and absence of 3 mM $MgCl_2$. *B*, quantified results plotted as percentage of maximal cross-linking determined at zero Ca^{2+} concentration. Mg^{2+} had no effect on maximal cross-linking. K_i values (μM) for Ca^{2+} inhibition of cross-linking of N30C-PLB to SERCA were 0.37 ± 0.05 and 0.46 ± 0.07 in the absence and presence of Mg^{2+}, respectively. K_i values for Ca^{2+} inhibition of PLB4 cross-linking were 1.52 ± 0.06 and 1.70 ± 0.10, respectively. Means ± S. E. from 3-5 determinations.

Figure 1

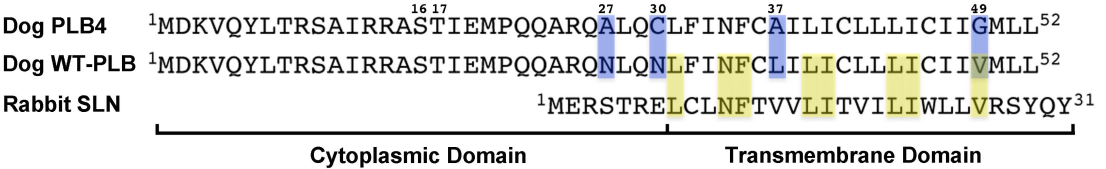
Dog PLB4 1MDKVQYLTRSAIRRASTIEMPQQARQALQCLFINFCAILICLLLICIIGMLL52
Dog WT-PLB 1MDKVQYLTRSAIRRASTIEMPQQARQNLQNLFINFCLILICLLLICIIVMLL52
Rabbit SLN 1MERSTRELCLNFTVVLITVILIWLLVRSYQY31
16 17
27
30
37
49
Cytoplasmic Domain
Transmembrane Domain

Figure 2

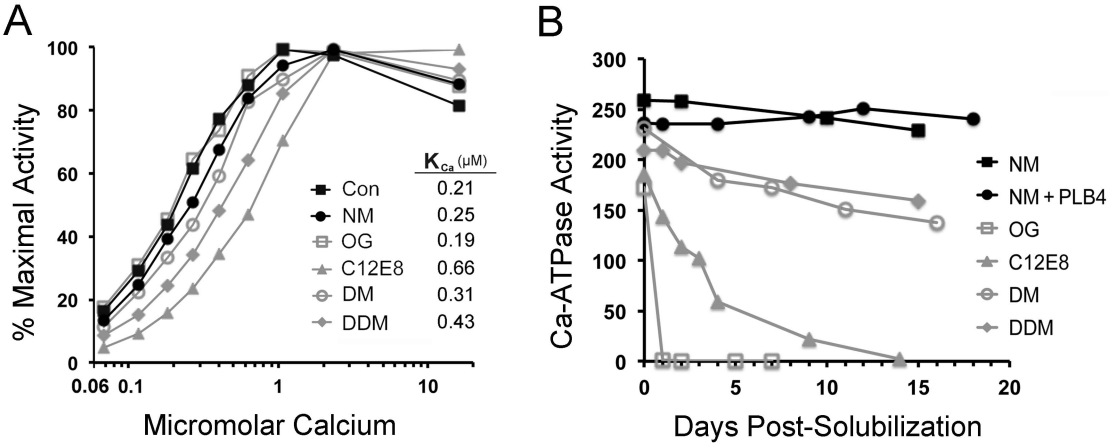
A
% Maximal Activity
Micromolar Calcium
0.06
0.1
1
10
0
20
40
60
80
100
K_{Ca} (μM)
Con 0.21
NM 0.25
OG 0.19
C12E8 0.66
DM 0.31
DDM 0.43
B
Ca-ATPase Activity
Days Post-Solubilization
0
50
100
150
200
250
300
5
10
15
20
NM
NM + PLB4
OG
C12E8
DM
DDM

Figure 3

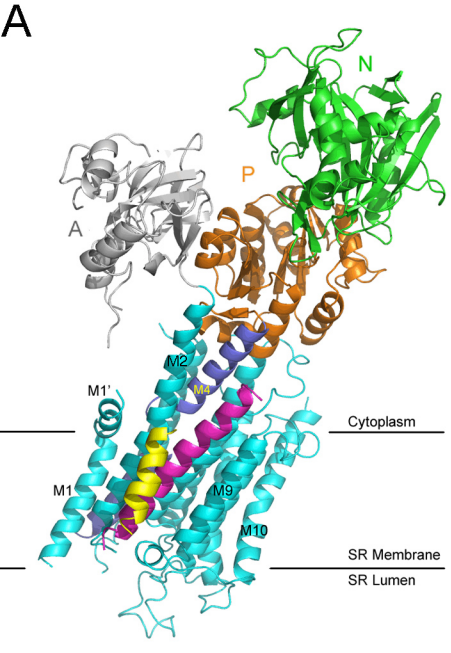
A
N
P
A
M2
M1'
M1
M9
M10
Cytoplasm
SR Membrane
SR Lumen

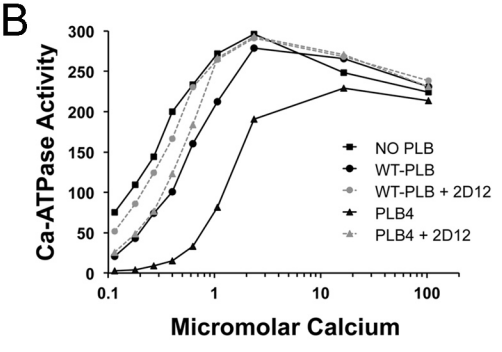
B
Ca-ATPase Activity
300
250
200
150
100
50
0
0.1
1
10
100
Micromolar Calcium
NO PLB
WT-PLB
WT-PLB + 2D12
PLB4
PLB4 + 2D12

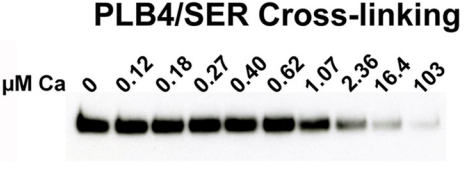
C
PLB4/SER Cross-linking
μM Ca
0
0.12
0.18
0.27
0.40
0.62
1.07
2.36
16.4
103

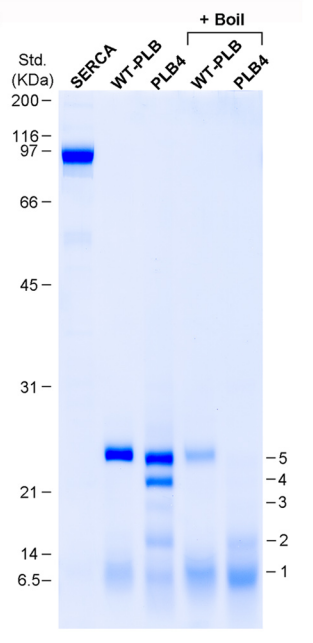
D
+ Boil
Std. (KDa)
SERCA
WT-PLB
PLB4
WT-PLB
PLB4
200
116
97
66
45
31
21
14
6.5
5
4
3
2
1

Figure 4

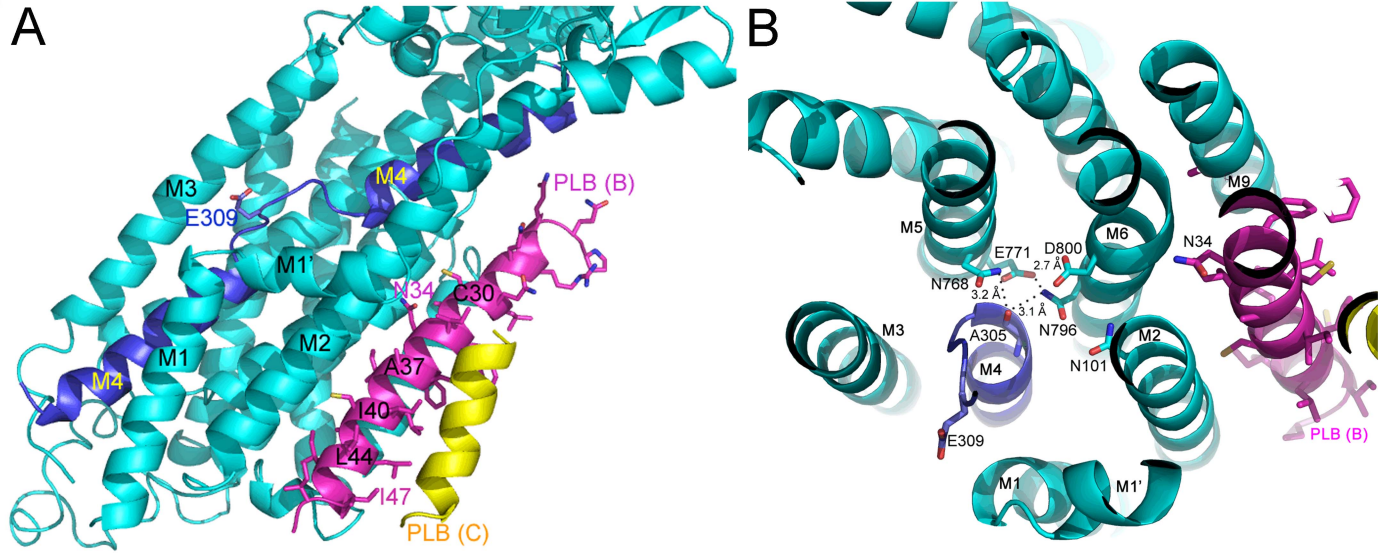
A
M3
E309
M4
PLB (B)
M1'
N34
C30
M2
M1
M4
A37
I40
L44
I47
PLB (C)
B
M5
E771
D800
M6
M9
N34
2.7 Å
N768
3.2 Å
3.1 Å
M3
A305
N796
M2
M4
N101
E309
PLB (B)
M1
M1'

Figure 5

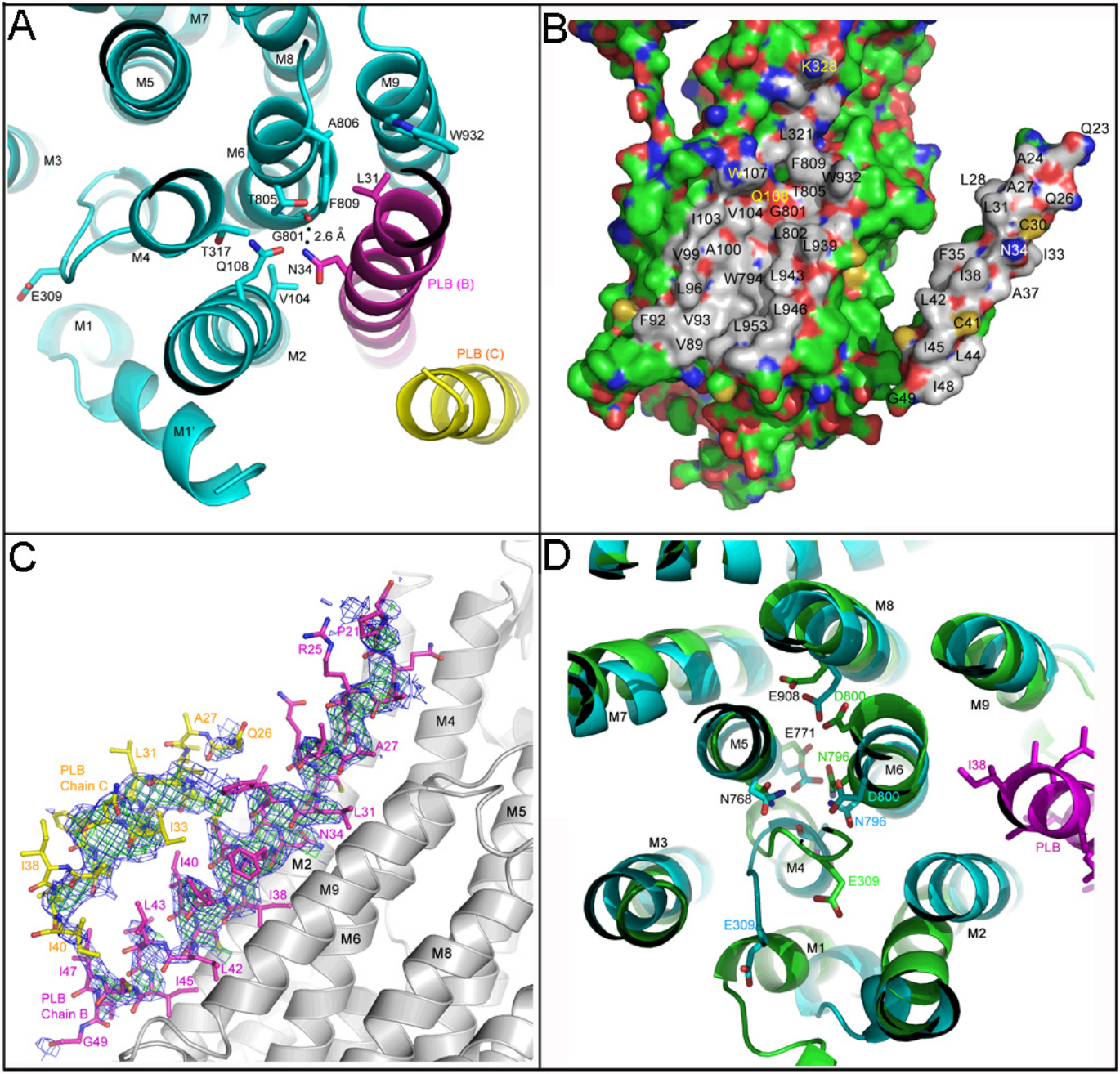
A
M7
M8
M5
M9
A806
W932
M6
M3
L31
T805
F809
G801
2.6 Å
T317
M4
Q108
N34
PLB (B)
E309
V104
M1
M2
PLB (C)
M1'
B
K328
L321
Q23
A24
F809
W107
W932
L28
T805
A27
Q165
Q26
I103
V104
G801
L31
C30
L802
L939
V99
A100
F35
N34
I33
W794
L943
I38
L96
A37
L946
L42
F92
V93
L953
C41
V89
I45
L44
I48
G49
C
P21
R25
A27
Q26
L31
PLB
Chain C
M4
M5
I33
N34
I38
I40
M2
M9
L43
I38
M6
M8
I40
I47
I45
L42
PLB
Chain B
G49
D
M8
E908
D800
M7
M9
M5
E771
N796
M6
N768
D800
N796
I38
PLB
M3
M4
E309
E309
M2
M1

Figure 6

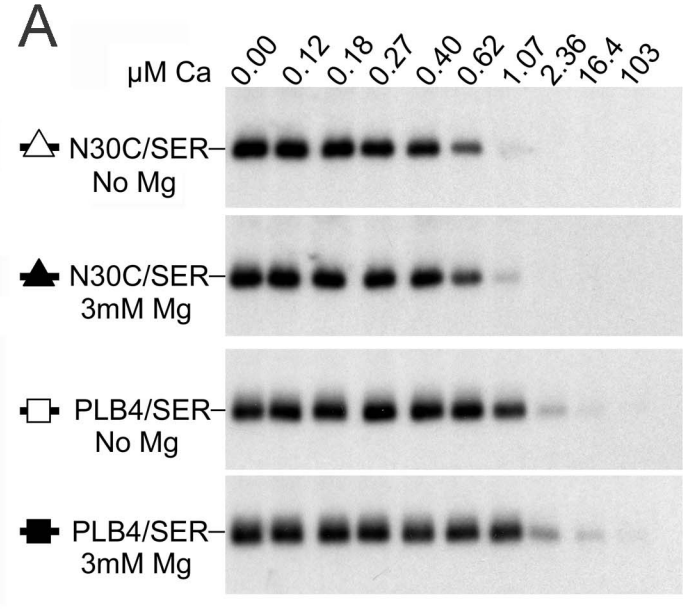
A
μM Ca
0.00
0.12
0.18
0.27
0.40
0.62
1.07
2.36
16.4
103
N30C/SER–
No Mg
N30C/SER–
3mM Mg
PLB4/SER–
No Mg
PLB4/SER–
3mM Mg

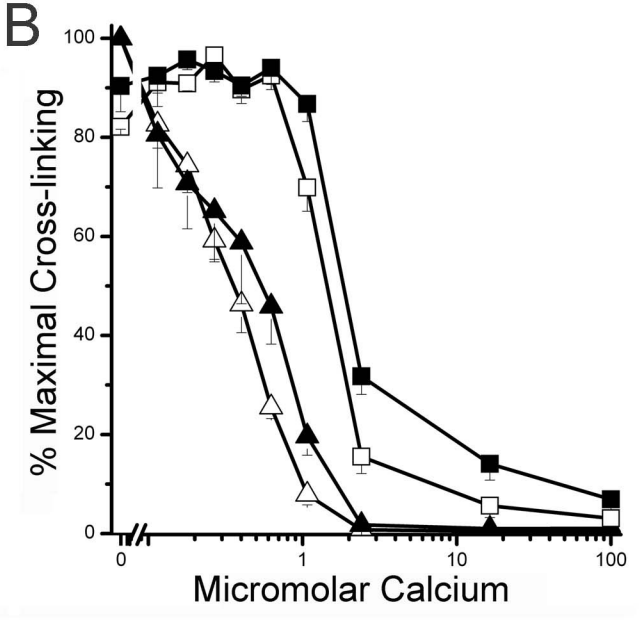
B
% Maximal Cross-linking
100
80
60
40
20
0
0
1
10
100
Micromolar Calcium

Membrane Biology:

The Structural Basis for Phospholamban Inhibition of the Calcium Pump in Sarcoplasmic Reticulum

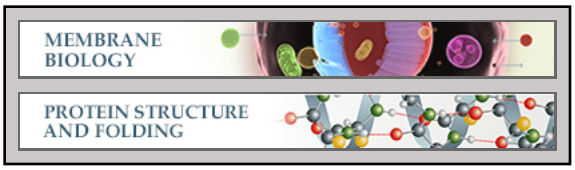

Brandy L. Akin, Thomas D. Hurley, Zhenhui Chen and Larry R. Jones

J. Biol. Chem. published online August 31, 2013

Access the most updated version of this article at doi: 10.1074/jbc.M113.501585

Find articles, minireviews, Reflections and Classics on similar topics on the JBC Affinity Sites.

Alerts:

- When this article is cited
- When a correction for this article is posted

Click here to choose from all of JBC's e-mail alerts

This article cites 0 references, 0 of which can be accessed free at
http://www.jbc.org/content/early/2013/08/31/jbc.M113.501585.full.html#ref-list-1